

## ON HELIUM 1083 NM LINE POLARIZATION DURING THE IMPULSIVE PHASE OF AN X1 FLARE

PHILIP G. JUDGE

High Altitude Observatory, National Center for Atmospheric Research,  
P.O. Box 3000, Boulder CO 80307-3000, USA; judge@ucar.edu

LUCIA KLEINT

Institute of 4D Technologies, University of Applied Sciences and Arts Northwestern Switzerland,  
5210 Windisch, Switzerland; lucia.kleint@fhnw.ch

ALBERTO SAINZ DALDA

High Altitude Observatory, National Center for Atmospheric Research,  
P.O. Box 3000, Boulder CO 80307-3000, USA; asainz@ucar.edu

## ABSTRACT

We analyze spectropolarimetric data of the He I 1083 nm multiplet ( $1s2s\ ^3S_1 - 1s2p\ ^3P_{2,1,0}^o$ ) during the X1 flare SOL2014-03-29T17:48, obtained with the Facility Infrared Spectrometer (FIRS) at the Dunn Solar Telescope. While scanning active region NOAA 12017, the FIRS slit crossed a flare ribbon during the impulsive phase, when the helium line intensities turned into emission at  $\lesssim$  twice the continuum intensity. Their linear polarization profiles are of the same sign across the multiplet including 1082.9 nm, intensity-like, at  $\lesssim$  5% of the continuum intensity. Weaker Zeeman-induced linear polarization is also observed. Only the strongest linear polarization coincides with hard X-ray (HXR) emission at 30-70 keV observed by the *Reuven Ramaty High Energy Solar Spectroscope Imager*. The polarization is generally more extended and lasts longer than the HXR emission. The upper  $J = 0$  level of the 1082.9 nm component is unpolarizable, thus lower level polarization is the culprit. We make non-LTE radiative transfer calculations in thermal slabs optimized to fit only intensities. The linear polarizations are naturally reproduced, through a systematic change of sign with wavelength of the radiation anisotropy when slab optical depths of the 1082.9 component are  $\lesssim$  1. Collisions with beams of particles are neither needed nor can they produce the same sign of polarization of the 1082.9 and 1083.0 nm components. The He I line polarization merely requires heating sufficient to produce slabs of the required thickness. Widely different polarizations of H $\alpha$ , reported previously, are explained by different radiative anisotropies arising from slabs of different optical depths.

*Subject headings:* Sun: atmosphere - Sun: chromosphere - Sun: flares - Sun: protons

## 1. INTRODUCTION

The physics of solar flares is still not understood in spite of over 80 years of quantitative research, arguably beginning with the work of Newton (1930) and Hale (1931). As reviewed by Benz (2008); Fletcher et al. (2011); Holman et al. (2011), flares are believed to originate from the slow buildup of magnetic energy in the corona, followed by sudden or “impulsive” energy release, most likely via reconnection (Carmichael 1964; Sturrock 1966; Hirayama 1974; Kopp & Pneuman 1976). But there remain elementary unanswered questions. For example, the origin of broad-band (“white light”) emission, observed for over 150 years (Carrington 1859), is still debated (Kerr & Fletcher 2014; Heinzel & Kleint 2014).

Given our rudimentary knowledge of flare physics, it is important to obtain critical observations. Here we analyze unusual polarimetric data of chromospheric He I 1083 nm multiplet ( $1s2s\ ^3S_1 - 1s2p\ ^3P_{2,1,0}^o$ ) observed during the impulsive phase of the X1 flare SOL2014-03-29T17:48. We study the origin of linear polarization  $P = \sqrt{Q^2 + U^2}$  (with  $Q$  and  $U$  the usual Stokes parameters) in this multiplet which have a peak magnitude  $|P|$  a few percent of intensity  $I$ . Kuckein et al. (2015a,b) report similar data for an M3.2 class flare with  $|P|/I$  an order of magnitude smaller, but with no analysis of the origin of the polarization.

Figure 1 shows images of the active region reconstructed from the FIRS scan during which the flare occurred, beginning at 17:40:06 UT on 29 March 2014, ending at 18:01:39 UT with Stokes  $I$  at 1083.0 nm and  $Q$  data, averaged over 0.1 nm. Each row of the image corresponds to one slit spectrum in FIRS, the lowest row shows the first spectrum, the next shows the spectrum acquired 13 seconds later, and so forth. Also shown are contours from the *Reuven Ramaty High Energy Solar Spectroscope Imager* (RHESSI, Lin et al. 2002). RHESSI records hard X-ray (HXR) emission which in flares is generally caused by accelerated electrons. Although the maximum polarization signal correlates with the maximum in HXR counts, lower levels of linear polarization are clearly visible where no HXR emission exists (e.g., near X=530”, Y=263”). These relationships will be discussed below, keeping an open mind as to the physical relationship between these measurements.

The X1 flare of 29 March 2014, like many flares, exhibits hard X-ray emission whose spectral properties in the standard model require supra-thermal electrons propagating down from the corona (e.g., Brown 1971; Fletcher et al. 2007). Such anisotropic distributions (“beams”) of particles can carry significant energy and momentum down to the solar atmosphere, from which white light emission seems to originate. Anisotropic particle distributions can induce “atomic po-

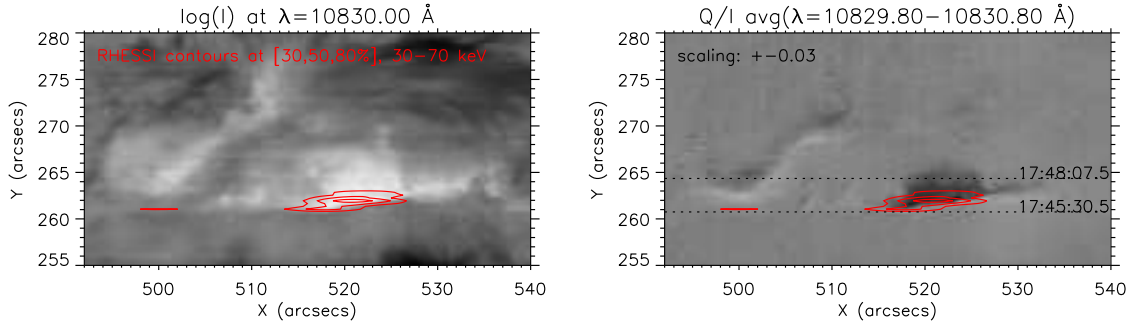


**Figure 1.** Context maps of Stokes  $I$  and  $Q$  of the He I 1083 nm multiplet are shown, each row in each image corresponding to one integration. The horizontal dashed lines span positions of the FIRS slit between the times shown, as it scanned from S to N on the plot. HXR RHESSI contours at [30,50,80]% of the peak flare intensity are plotted on top of the He intensity  $I$  (left panel) and linear polarization  $Q$  (right panel). The strongest HXR emission coincides with the strongest polarization, but significant polarization is seen outside areas detected by RHESSI.

larization” which in turn generates spectral line polarization (Percival & Seaton 1958). Observations in the Balmer- $\alpha$  line of hydrogen at 656.3 nm during flares have been made to seek evidence for such anisotropies (Henoux & Chambe 1990; Henoux et al. 1990; Hanaoka 2003; Bianda et al. 2005). But as yet there is no consensus on properties of  $H\alpha$  polarization from flare ribbons. In part this is because ribbons are difficult to observe with a spectrograph because flares are not predictable.  $H\alpha$  sometimes has  $P/I$  at a level of a 5 percent (Hanaoka 2003). At other times, and with different instruments, it appears to show no polarization, with  $P/I < 0.5\%$  (Bianda et al. 2005). Different flares behave differently. The polarized spectrum can depend on the phase of flare evolution, on the distance of the flare from disk center, on the strength of the flare, the configuration of the magnetic field, among the possibilities. Polarimetric observations themselves also use diverse spectral lines, different instruments (gratings and/or filters), under different angular resolution, seeing and cross-talk conditions. Thus the diversity of  $H\alpha$  polarized light from flares is not surprising, but it is large and the origin of the differences are not known.

Atomic polarization is generated also under conditions of asymmetry in the radiation fields (e.g., Casini & Landi Degl’Innocenti 2008). In the present work we examine the helium data with the aim of identifying the origin of the polarization. The He I 1083 nm multiplet has advantages over  $H\alpha$ : fine structure is partly split in solar spectra – it consists of just three lines (two blended at 1083.025 and 1083.034 nm, and the 1082.909 nm line<sup>1</sup>), there is no additional complexity from hyperfine structure, and, importantly, the  $J = 0$  upper level of the 1082.909 nm transition is intrinsically unpolarizable. In Figure 2 we show this multiplet’s levels along with the long-lived levels of helium, in a highly simplified term diagram.

## 2. ANALYSIS

### 2.1. Observations

We obtained spectropolarimetric data with the Facility Infrared Spectrometer (“FIRS” Jaeggli 2011) at the Dunn Solar Telescope (“DST”) of the National Solar Observatory in Sunspot, New Mexico. In our recent paper

<sup>1</sup> <http://www.nist.gov/pml/data/asd.cfm>

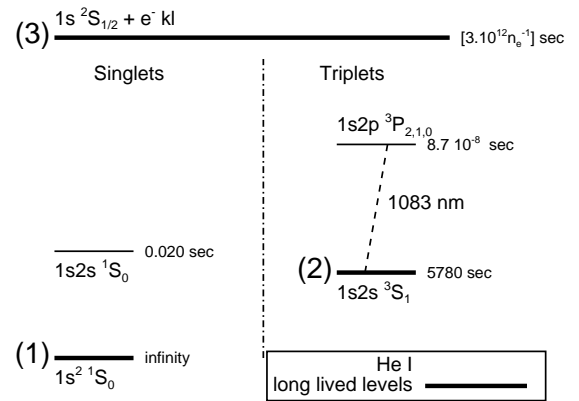


**Figure 2.** Energy levels of He I are shown, including the long-lived levels and the levels between which the 1083 nm transitions occur. The lifetimes of the levels are listed along with the leading terms in the wavefunctions appropriate for each level. The lifetime of the He II ground level is infinite *in vacuo*, the lifetime listed is the recombination time for a  $\text{He}^+$  ion embedded in a plasma with electron density  $n_e$  for temperatures near  $10^4$  K.

(Judge et al. 2014, henceforth “Paper I”), we reported observations of the footpoint of the X1 flare SOL2014-03-29T17:48 in active region NOAA 12017. In Paper I we analyzed the continuum and line of Si I at 1082.7 nm with the aim of explaining an associated sunquake. Here we analyze new reductions of the same scans but focusing on the He I 1083 nm multiplet.

Figure 3 shows data from one slit position obtained in the flare ribbon during the impulsive phase, from one integration from 17:46:42 – 17:46:55 UT. Wavelength is along the abscissa, position along the slit on the ordinate. The peak of the He I emission arises from  $X = 520''$ ,  $Y = 264''$ , close to the brightest part of the flare seen at other infrared wavelengths (Paper I). The three vertical lines show the approximate rest positions of the He I 1083 nm multiplet. The strong absorption line of Si I lies along  $X = -0.3$  nm, the line core also goes into emission near  $Y = 37$ . The Si I line exhibits Stokes  $Q$ ,  $U$  and  $V$  profiles which are proportional to second and first derivatives with wavelength of Stokes  $I$  respectively. These profiles arise from the Zeeman effect (e.g. Jefferies et al. 1989; Lites 2000).

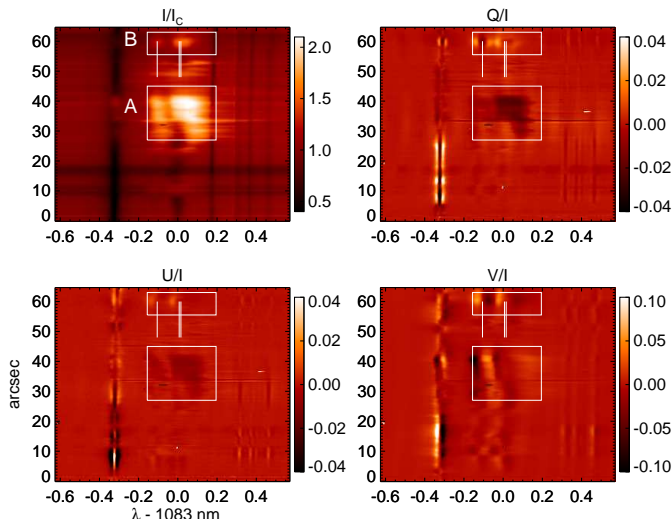


**Figure 3.** Stokes profiles are shown for one slit position of FIRS acquired over the 13 seconds after 17:46:42 UT. Wavelength increases from left to right (each pixel is 0.0039 nm, 39 mÅ), and the ordinate measures position from W to E along the projected slit in units of  $0''.3$  (the zero point is arbitrary). The three vertical lines show the three transitions of He I, the two rightmost are blended. The boxed regions highlight the bright footpoint that also shows the unusual profiles of  $Q$  and  $U$ . “A” and “B” mark footpoint emission areas, for comparison with later figures.

Figure 3 shows Stokes profiles as a function of wavelength and position along the FIRS slit, during the flare’s impulsive phase.

Unlike the Si I line, the He I impulsive phase spectra show signatures of strong atomic polarization, with Stokes  $Q$  and  $U$  profiles giving a polarization  $P/I$  which is several percent of the intensity,  $I$ , during the flare. The impulsive phase linear polarization in the He I 1083 nm multiplet has profiles similar but not identical to Stokes  $I$ , with peak signal-to-noise ratios of at least 20. The “reference direction for linear polarization” was E-W on the solar disk (i.e. positive  $Q$  goes from E to W).

## 2.2. Data reduction

We re-reduced the FIRS data reported in Paper I using the official NSO software package written by C. Beck (<http://nsosp.nso.edu/dst-pipelines>). The new reductions process the data minimally to optimize the purity of the polarization signals. In particular, the flat fielding algorithm makes no assumptions concerning the solar line profiles of interest, and the polarimetric calibration includes a correction of  $I \rightarrow [Q, U, V]$  cross-talk using continuum pixels which we assume, to the sensitivities we achieve ( $P/I \approx 10^{-3}$ ), are polarization-free.

In Paper I we measured noise levels of  $8 \times 10^{-4} I_C$ , where  $I_C$  is the median pre-flare continuum intensity. However, the reduced polarization data contain obvious optical fringes, the largest of which are seen in Stokes  $V$ , at the level of  $2 \times 10^{-3} I_C$ . These fringes are not insignificant when discussing the He I  $Q, U, V$  spectra. We tried and failed to remove fringes using the PCA-based algorithm of Casini et al. (2012b). We simply could not make the fringes belong only to one set of components and the solar data to another, orthogonal set. Instead, for wavelengths close to the He I 1083 nm multiplet, we noted that almost no polarization was detectable in the

first and last slit positions of the scan during which the flare occurred. By assuming that these data only contain fringes and other slowly varying artifacts, we made a linear interpolation in time between the first and last scans for  $Q, U$ , and subtracted the interpolated data from the  $Q, U$  spectra. While not perfect, the procedure removed the bulk of the fringe pattern (compare Figure 3 with Figure 2 of Paper I.) However there remain artifacts visible as diffuse vertical stripes in the center of the Stokes  $Q$  panel of Figure 3. This is unfortunate since the linear polarization of the 1082.9 and 1083.0 nm components of the He I 1083 nm multiplet is expected to show both positive and negative  $Q$  and  $U$  (section 3).

No polarization is visible in the telluric line of  $H_2O$  lying along the column near 1083.2 nm in Figure 3. The upper limit to any polarization at these wavelengths is below  $10^{-3} I_C$ , far less than the  $\gtrsim 10^{-2} I_C$  values of  $Q$  and  $U$  found during the flare scan. Thus, at the wavelengths of the telluric line, errors in the polarization calibration are significantly smaller than the  $Q, U$  signals we are trying to obtain from these data. However, this encouraging analysis cannot naively be applied to every wavelength in the spectrum in the presence of seeing- or evolutionary-driven crosstalk for reasons given in Appendix A.

During the impulsive phase, the He I lines also show hints of Zeeman-induced patterns near  $Y = 60''$  (box “B”). But the He I polarization is strikingly different in the region of strong flare emission in the region  $25'' < Y < 41''$  where  $Q$  and  $U$  profiles appear similar to  $I$ . These extent of profiles *across* the slit is naturally mixed with the time-dependent stepping of the FIRS slit. The  $I$ -like  $Q$  and  $U$  profiles seen in region “A” were observed mostly in the 9 scans acquired between 17:46 and 17:48 UT, covering  $2.7''$ . Figure 4 shows samples of these spectra. In Appendix A we argue that the measurements are mostly of solar origin.

The RHESSI data of Figure 1 were processed as follows. We reconstructed CLEAN images (Hurford et al. 2002) for each duration of a FIRS raster step (12 s) for the 30-70 keV range of RHESSI. The resulting maps were then rolled by 0.2 degrees to align RHESSI to FIRS (which was aligned to SDO/HMI, Kleint et al. 2015). We then constructed a “RHESSI raster”, simulating what it would have recorded, had it scanned across the solar surface like FIRS. For each solar  $Y$  coordinate of a FIRS raster step, the RHESSI reconstructed intensities at that time and location were saved in a new map. Thus, only those contours above 30% of the newly constructed map were plotted in Fig. 1, to avoid low intensity artifacts arising from the CLEAN algorithm. This imperfect treatment of RHESSI data serves to try to illustrate the locations of the HXR emission from a sequence of RHESSI CLEAN images.

## 2.3. A simple model for the He I-emitting plasma

Figure 5 shows profiles from two representative points. Dashed lines show data from outside of the bright ribbon, solid lines those from within the ribbon itself. Let us consider the ribbon emission during the impulsive phase. Under optically thin conditions, the intensity ratio between the blended 1083.0 and single 1082.9 components will be the ratio of the statistical weights of the upper levels, i.e.,  $(5 + 3) : 1 = 8 : 1$ , whether in emission or

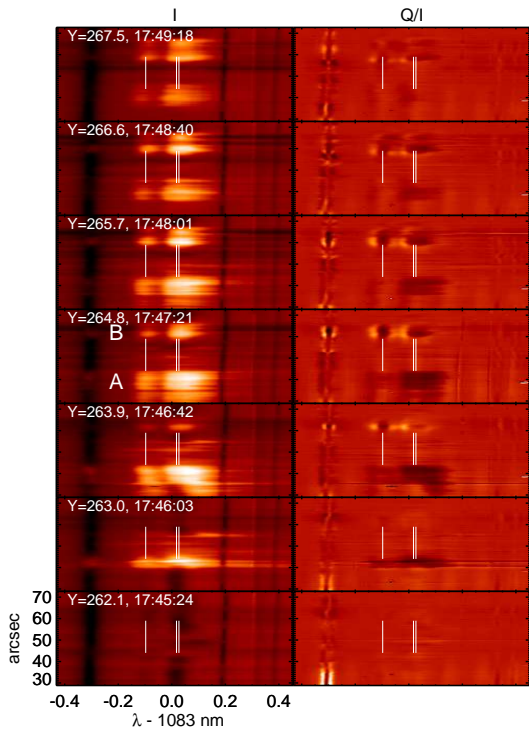


**Figure 4.** Stokes  $I$  (left) and  $Q$  (right) profiles are shown for seven positions of the FIRS slit on the Sun, each integrated during the 13 seconds after the times shown, which are separated by 40 s. The solar  $Y$  position of the slit is listed along with the times, which can be seen in Figure 1. The scales and intensities of the images are byte scaled to the same ranges shown in Figure 3.

absorption.

Care must be taken in analyzing the intensity profiles, a naïve inspection of the profile indicates the peak near 1082.9 contains roughly 1/8 of the energy of the 1083.0 peak. But the 1082.9 and 1083.0 nm components have very different intensity profiles, the 1083.0 component having an extended red wing. If we insist that the emission is optically thin we must conclude that the wavelength-integrated ratio is far less than the peak ratio of 1/8 because the 1082.9 component will have its own red wing emission sitting under the 1083.0 nm component. We therefore conclude that the intensity during the impulsive phase is *incompatible with the optically thin ratio of 8:1. The emitting plasma is therefore optically thick in at least the 1083 nm components.*

We estimate the optical depth of the He I emitting plasma using a parameterized non-LTE slab model. Such a simple model is appropriate for the problem at hand, a slab geometry being similar to the kind of structures in the middle-upper chromosphere found in beam-heated hydrodynamic flare models (e.g., Allred et al. 2005). The flare ribbons seen in He I 1083 nm multiplet extend over areas of  $\approx 30$  square arcseconds, with horizontal scales of a few thousand km, much larger than the 100km thickness of slabs in such flare models. Instead of solving multi-level non-LTE rate equations we adopt a line source function  $S_L$  for a two-level atom and we iterate between this linear equation (1) and the transfer equation (2):

$$S_L = \epsilon B + (1 - \epsilon)\bar{J}. \quad (1)$$

$$\bar{J} = \Lambda[S_L]. \quad (2)$$

Here, both  $B$  and  $\epsilon$  are assumed constant for each slab,  $B$  is the Planck function (temperature) within the slab,  $\epsilon = C_{21}/(C_{21} + A_{21})$  where  $C$  and  $A$  are collisional and spontaneous decay transition probabilities between the two levels. The variable  $\bar{J}$  is the mean intensity averaged over the absorption line profile. Equation (2) gives the solution to the transfer equation for a given  $S_L$ , computed using a lower boundary representing the photosphere as a Planck function with temperature 5700 K, and an the upper boundary having no incoming radiation. (The “ $\Lambda$ ”-operator (2) integrates over depth, over three slant angles to the slab normal, and over frequencies where the line has some opacity). Lambda iterations were used to bring these equations to convergence using a Feautrier solver, because the optical depths derived were modest,  $\lesssim 20$ .

Although the 1083nm multiplet involves transitions between four levels, a two-level atom suffices under conditions of source function equality in multiplets (Mihalas 1978). Using a genetic algorithm (GA) we searched the parameter space for values of the slab optical depth, the non-LTE parameter  $\epsilon$  and the Planck function (i.e., temperature) of the slab plasma. At the same time we searched for two unresolved plasma “elements” (to avoid confusion with different line “components” we call these “elements”) giving line profiles inside the slab, keeping the opacity ratios fixed to the atomic values for the three lines. These elements are defined by their relative opacity, the line widths and Doppler shifts. It is clear from the emergent  $I$  profiles (Figure 5) that at least two elements are needed, one to account for the relatively narrow 1082.9 nm peaks and another for the extended red wing and broader peak of the 1083.0 nm components.

Results of the non-LTE intensity calculations are shown in Figure 6. The top left panel shows the intensity data from the center of box “A” in Figure 3. The dashed line shows the optimal fit from the slab calculations, and the dot-dashed line shows the run of opacity with wavelength from the two elements combined in the He I 1083 nm multiplet. The line center optical depth of the fitted slab is 15,  $\epsilon = 0.011$  and the Planck function is 10 times the Planck function in the photosphere. All intensities shown in the figure are divided by the photospheric Planck function. The role of the finite optical depths is seen in the GA solution (dashed line) that is far broader than the elementary opacity itself. The solution is also slightly self-reversed at the peak intensity. The GA’s solution is very different from the dot-dashed opacity which would represent the solution under optically thin conditions: the ratio of the 1082.9 to 1083.0 components being closer to observations in the case of finite optical depth.

#### 2.4. Origin of the Impulsive Phase Linear Polarization

To produce emission line intensity from atoms in a solar plasma, the environment must generate a finite *population* in a given level, for example by impact with electrons or by irradiation. To produce polarization, the environment must introduce anisotropy to break symmetries often present under natural conditions (such as in thermal equilibrium, or LTE in cylindrically-symmetric geometry). In the spherical tensor basis (Fano 1957), spectral line polarization requires non-zero atomic *alignment* and/or atomic *orientation*



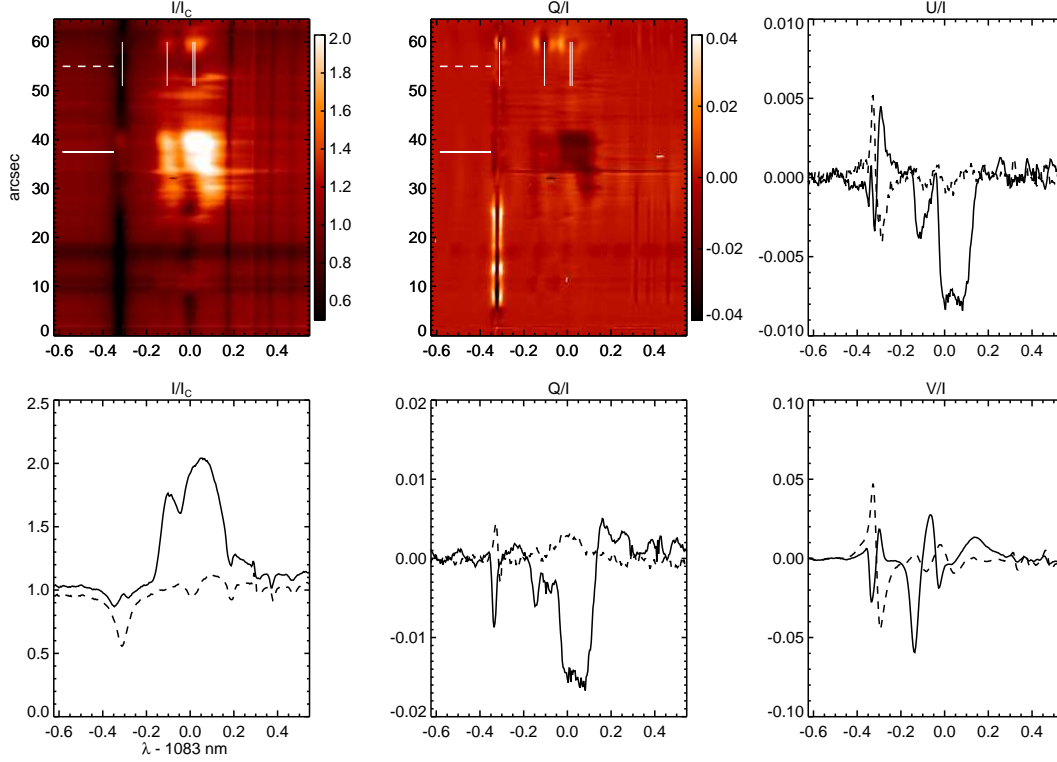


**Figure 5.** Line plots of Stokes  $I$  and  $Q, U, V$  profiles are shown along with  $I, Q$  images shown earlier. All plots are divided by the intensity. The 1082.7 nm line of Si I is marked as a vertical line in the images, along with the three lines of the He I 1083 nm multiplet to the right. Dashed lines show the Stokes profiles for  $Y = 5''$ , and solid lines profiles for position  $Y = 38''$  during the bright impulsive phase.

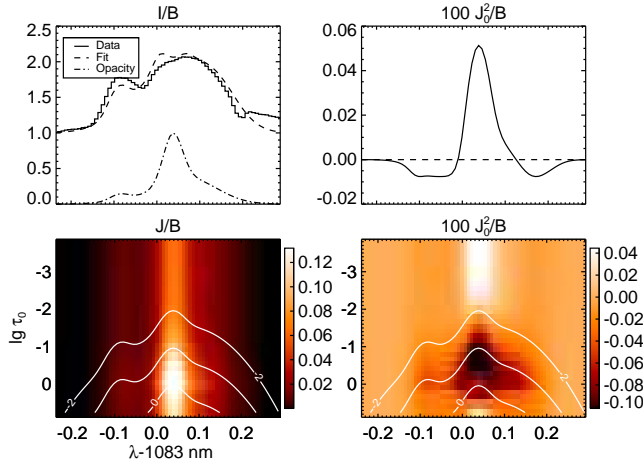


**Figure 6.** Results of non-LTE radiative transfer calculations in a slab are shown in which the slab parameters were optimized to fit the observed intensities (top left panel) from position  $Y = 41''$  from Figure 3, part of the bright flare ribbon. The model slab has an optical depth at the line core of 15, a source function with a thermal contribution of  $\epsilon B$  where  $\epsilon = 0.011$  and a local emission term with  $B = 10 \times$  the 5700K photospheric Planck function, corresponding to a temperature of  $2 \times 10^4$ K. The upper right panel shows the radiation anisotropy as a function of wavelength emerging from the top of the slab, the lower panels expand the mean intensity and anisotropy as a function both of wavelength and optical depth in the slab (the solar photosphere lies just beneath the bottom of these plots, represented by upcoming radiation which is a Planck function at 5700K, independent of slant angle). Contours mark logarithmic values of monochromatic optical depth.

(Landi Degl’Innocenti & Landolfi 2004) of atomic levels. Atomic population, alignment and orientation lead to intensity, linear and circular polarization in spectral lines respectively. For He I three long-lived atomic levels need

be considered as reservoirs from which significant population, alignment and orientation can be produced (Figure 2). Note that the linear polarization that we seek to explain has a magnitude that is of the order of the circular polarization and very different spectral and spatial profiles (Figure 3). Thus we look to mechanisms that generate alignment from asymmetries and ignore possible orientation-to-alignment effects.

We first examine radiative anisotropies and discuss collisional polarization in Appendix B. In the natural basis of spherical tensors (Fano 1957), the lowest order term influencing linear polarization is the tensor component of the mean (i.e., wavelength-averaged) intensity  $J_Q^K$  with  $K = 2$  and  $Q = 0$  (e.g. Casini & Landi Degl’Innocenti 2008). The mean intensity  $J_0^0$  and the term  $J_0^2$  are, under the cylindrical symmetry present in the slab (Landi Degl’Innocenti & Landolfi 2004, equation 5.164),

$$J_0^0 = \frac{1}{2} \int_{-1}^{+1} I(\mu) d\mu \quad (3)$$

$$J_0^2 = \frac{1}{4\sqrt{2}} \int_{-1}^{+1} (3\mu^2 - 1) I(\mu) d\mu \quad (4)$$

where  $\mu = \cos \theta$  with  $\theta$  the angle of the ray to the normal of the slab. Generally speaking,  $J_0^2$ , when averaged over the absorption line profile, is a radiative source term for linear polarization (see equation 5). The right uppermost panel of Figure 6 shows  $J_0^2$  just above the slab (which consists only of outward directed radiation). The lower panels show  $J_0^0$  and  $J_0^2$  as functions of wavelength across the 1083nm region and depth in the slab. It is clear that *with slab optical depths*  $> 1$ , *radiation anisotropies*

in He I 1083 nm multiplet can readily approach a few percent of the mean intensities. Also, an optically thick 1 dimensional slab generates  $J_0^2$  values which change sign with wavelength, in particular between the 1082.9 and 1083.0 nm components.

Given the three reservoirs of population, two radiative processes can be important for the He I 1083 nm multiplet. The first is photoionization by photons below 50.4 nm from level 1 to 3, leaving level 3 to be impacted by electrons to produce population in the  $1s2p\ ^3P_{2,1,0}^o$  level via recombination and cascades. Level 3, with  $J = 1/2$ , is intrinsically unpolarizable for  $^4\text{He}$  isotopes. Thus to produce any atomic alignment in a  $1s2p\ ^3P_{2,1}^o$  level through photoionization followed by recombination requires an anisotropic distribution of captured electrons (i.e., electrons  $e^-(k\ell)$  with energy  $k$  and angular momentum  $\ell$  cannot be drawn from an isotropic distribution). This origin of polarization is therefore collisional, which discussed separately in Appendix B.

The second radiative process to consider is photo-excitation from level 2 to  $1s2p\ ^3P_{2,1,0}^o$ , i.e. photo-excitation in the He I 1083 nm multiplet itself, or to higher levels in the triplet system that by radiative cascade transfer alignment to the  $1s2p\ ^3P_{2,1}^o$  levels themselves. For our purposes it suffices to ignore cascade contributions to alignment and orientation. The simple non-LTE radiation transfer slab model used above yields the needed anisotropy of the radiation field in the He I 1083 nm multiplet at a level of a few percent. But these values are merely in the radiation field, related to but not identical to the Stokes components that emerge from the radiating helium atoms. The radiative transfer determining the actual polarization in the three transitions is considerably more complex than the two-level atom discussed here (Casini & Landi Degl’Innocenti 2008, section 12.4), especially because the  $J = 1$  lower level is polarizable. However, the slab and two-level approximation for the linear polarization yields the right order of magnitude for the atomic polarization as we can see from the following. The simplest possible case is a two-level atom with an unpolarizable lower level, the solutions to which yield (Landi Degl’Innocenti & Landolfi 2004, equations 10.50 and 10.51):

$$\sigma_0^2 = \frac{D_{JJ_0} \bar{J}_0^2}{\epsilon B_\nu(T) + \bar{J}_0^0} \times \frac{1 + \epsilon}{1 + \epsilon + \delta_u^{(2)}}, \quad (5)$$

where  $\sigma_0^2$  is the ratio of atomic alignment to atomic population for the upper level,  $D_{JJ_0}$  (of order 1) depends only on the quantum numbers of the two-level atom,  $\epsilon$  is the ratio of the downward (super-elastic) collision rate to the Einstein A-coefficient,  $B_\nu(T)$  is the Planck function at the coronal temperature  $T$ , and  $\delta_u^{(2)}$  is the depolarizing collisional rate of the upper level.  $\sigma_0^2$  is the leading term in contribution to the fraction of linearly polarized light, it is linearly proportional to the frequency averaged value,  $\bar{J}_0^2$ . With small values of  $\epsilon$ ,  $\epsilon B_\nu(T)/J_0^0$  and  $\delta_u^{(2)}$ ,  $\sigma_0^2$  becomes  $\approx \bar{J}_0^2/\bar{J}_0^0$ . In words, the ratio of alignment to population is  $\approx \bar{J}_0^2/\bar{J}_0^0$ , so that the observed ratio  $P/I$  is also  $\approx \bar{J}_0^2/\bar{J}_0^0$ .

By examining various slab models, we find that the primary source of atomic polarization in the He I 1083 nm

multiplet is from non-zero values of  $J_0^2/J_0^0$  generated naturally scattering in slabs which have an optical depth  $\tau_0$  in the core of the strongest lines of at least 1. At smaller optical depths the radiation field is modified weakly by the helium lines and we see almost pure photospheric continuum, which far from the solar limb is very weakly polarized ( $P/I_C < 0.0001$ , Stenflo et al. 1997). The best fits to the observed intensity profiles, such as that shown in Figure 6, produce linear polarization of a few percent when slabs have 1083.0 nm optical depths  $\approx 10^1$ . In such models  $J_0^2/J_0^0$  changes sign from  $< 0$  at wavelengths where the slab is optically thin, to  $> 0$  for wavelengths where it is optically thick. Since the same sign of  $J_0^2/J_0^0$  generates polarization in the 1082.9 nm component that is of opposite sign to those in the 1083.0 components (table 10.3 of Landi Degl’Innocenti & Landolfi 2004), the effect is to generate polarization of *the same sign for all three components* under the conditions shown in the right panels of Figure 6. If the optical depth varies from place to place in the flare ribbons, the linear polarization will vary accordingly. In particular, optically thin slabs will show very little polarization even though they might even have comparable intensities. This picture appears broadly compatible with the diverse observations reported here and in Kuckein et al. (2015a,b), which have  $P/I \approx 0.1\%$ .

From the definition of Stokes vectors, the electric vector of the polarized radiation lies along the direction in which, when rotated to a frame rotated on the plane-of-sky, Stokes  $U$  becomes zero. This places the electric vector along the direction  $\frac{1}{2} \arctan U/Q$ , which for the 1083.0 nm component is  $\approx 15^\circ$  wrt the E-W direction. Observed  $U/Q$  ratios seen during the flare are close to  $1/2$ . Since the polarization has a radiative origin, and the magnetic field strengths of several hundred G (paper I) greatly exceed the ‘‘Hanle’’ field strength which for 1083nm is close to 1G (Casini & Landi Degl’Innocenti 2008), the electric vector under this condition has a  $90^\circ$  ambiguity. Sun center is at  $30^\circ$  to the E-W direction, The Si I Zeeman patterns from paper I place the underlying photospheric field close to the Sun center direction, with a statistical fluctuation of around  $40^\circ$  in the pre-flare footpoints. Our conclusion is that the electric field vector probably lies parallel to the magnetic field in the plane of the sky, not perpendicular to it. This simply means that the atomic alignment for the 1083nm component is positive, which is entirely consistent with the calculations presented above (Figure 6).

Štěpán & Heinzel (2013) calculated polarization in a stratified atmosphere assuming a two dimensional geometry to study effects of asymmetries in radiation at the *edges* of flare ribbons. Our slab calculations are consistent with theirs away from the regions of strong horizontal gradients. Positive alignments are found within ribbons which have a physical width  $\gg \lambda$  where  $\lambda$  is a local photon mean free path, and where transport is essentially only vertical. We note that  $\lambda$  is expected to be on the order of a pressure scale height, perhaps  $10^2$  km, far smaller than the ribbon’s width of 3 Mm or more (Figure 1). Our work differs from Štěpán & Heinzel (2013) mainly through our assumption of a slab, and by the fact that we look at all three components of a multiplet sampling very different optical depths. The change in sign of

alignment between the 1083 and 1082.9 nm components implied by Figure 6 is an entirely new and unexpected result.

Finally, in Appendix B we review collisional origins of the He I 1083 nm multiplet, assuming that energetic particles responsible for HXR emission are anisotropic and that they directly generate atomic polarization (e.g. Henoux & Chambe 1990). Collisions cannot by themselves produce polarization in 1082.9 nm, this requires the same lower-level polarization via radiation transfer outlined above. They also cannot readily account for the spatio-temporal differences between the HXR and helium polarization data shown in Figure 1. We conclude, based upon collisional relaxation times, that any direct contribution to the polarization from anisotropic particles most likely would have to arise from protons near 1 MeV. Given the success of the radiative models above though, there is no reason to invoke collisions to explain the data.

### 3. DISCUSSION AND CONCLUSIONS

We have analyzed data for the He I 1083 nm multiplet during the X1 class flare SOL2014-03-29T17:48. We found that the He I profiles are formed in an optically thick layer lying above the solar photosphere. The peculiar  $Q$  and  $U$  Stokes profiles are dominated by a real solar signal. The most probable origin of the observed linear polarization during the impulsive phase is *anisotropic photon scattering in a slab of optical depth of order 10*, somewhere above the photosphere, with no need to invoke collisionally-induced anisotropy. The high energy electrons required to explain the HXR emission seen with RHESSI serve not as a direct cause of atomic polarization through collisions from an anisotropic electron population, but merely as a source of energy that, as it thermalizes, generates thermal emission from the slab.

A remarkable and unanticipated success of this simple model is the fact that it predicts that the 1082.9 nm and 1083.0 nm components will have the same sign, as observed. Under previously discovered conditions in prominences and filaments, lower level polarization in the 1082.9 nm component leads to linear polarization of the opposite sign to the polarization seen in the 1083.0 components (Trujillo Bueno et al. 2002). However, here the observations clearly reveal the same sign of polarization in the entire multiplet. The explanation lies in the change of sign of the anisotropy,  $J_0^2$  between these two components (top right panel of Figure 6). This sign change arises naturally from the slab geometry under the presence of significant thermal emission from the slab itself, and when the strongest 1083.0 nm components have optical depths of order ten, with the 1082.9 nm component having optical depth of order one.

The impulsive phase of the flare thus appears to heat the upper chromosphere sufficiently to produce emission in the entire He I 1083 nm multiplet and at the same time the fit to the intensity spectrum leads naturally to conditions where the three components must have the same sign in linear polarization. This is also, perhaps, a hint that the far red wing of the 1083.0 nm component shows a negative polarization (see the lower middle panel of Figure 5), but we remind the reader that the polarization fringes are not negligible in comparison

with these weak signals (see the diffuse regular vertical stripes in the upper middle panel). In Appendix B we argue that collisional impact polarization is unlikely to produce the linear polarization observed. In fact, the 1082.9 nm transition cannot be polarized without lower level polarization. It is difficult to see how this can be produced effectively by collisions alone.

To test this conclusion further we suggest the following. First, we must obtain the highest sensitivity data possible for additional impulsive phases. Second, we must have a strategy to reduce instrumental artifacts such as fringes. If we can obtain reliable data with a sensitivity of  $P/I \lesssim 10^{-3}$  with negligible residual systematic errors, then we can seek the presence of the predicted change of sign in linear polarization between the 1083.0 and 1082.9 nm components that must arise from the multi-level transfer in slabs of optical depths greater than one (see figure 12.16 of Casini & Landi Degl’Innocenti 2008). Third, we must develop a radiative transfer program to handle the non-LTE radiation fields and density matrices for the radiating atom at least in slabs. Section 12.4.2 of Casini & Landi Degl’Innocenti (2008) presents an initial model based upon two-level atoms, with lower (upper) levels with  $J = 0$  (1) and 1 (0) respectively. The latter case exhibits the lower level polarization or “dichroic polarization” observed in a filament of finite optical depth (Trujillo Bueno et al. 2002), with the tell-tale change in sign of polarization between the 1083.0 and 1082.9 nm components that characterize transfer through a slab of optical depth  $\gtrsim 1$ . Unfortunately, the residual fringes and crosstalk present in our data confuse this critical aspect of our particular data.

If we are later proven incorrect, and collisions are important for generation of He I 1083 nm multiplet polarization, there will be additional implications. Conflicting constraints on the energy needed to produce polarizing electron-helium collisions suggests that instead *protons* might conceivably cause some polarization seen at the footpoints of this X1 flare. In this picture, the polarization is generated by an anisotropic distribution of protons of  $\approx 1$  MeV impacting the top of the chromosphere see also Henoux et al. 1990.

Finally, the diverse results in the literature regarding the  $H\alpha$  (Henoux & Chambe 1990; Henoux et al. 1990; Hanaoka 2003; Bianda et al. 2005) and now He I 1083 nm multiplet polarization (compare our measurements with those of Kuckein et al. 2015a,b) can readily be explained once the optical depth of a slab is recognized as a primary determinant of the outgoing polarized light. This is a quite different model from an earlier picture where anisotropically distributed particles are responsible for linearly polarized light from chromospheric spectral lines (Henoux et al. 1990).

Data in this publication were obtained with the facilities of the National Solar Observatory, which is operated by the Association of Universities for Research in Astronomy, Inc. (AURA), under cooperative agreement with the National Science Foundation. Part of this work was carried out under NASA grants NNX13AI63G and NNX14AQ31G. We thank the observers at the DST for their help and Javier Trujillo Bueno, Fatima Rubio de Costa and Marina Battaglia for helpful discussions.

Christian Beck was extremely helpful in demonstrating usage of the NSO data reduction package. We acknowledge other helpful discussions that took part at ISSI.

## APPENDIX

### A. TIME VARIATIONS, FLARES, AND CROSSTALK

Here we review origins of errors in the measurement process that arise because light coming into spectropolarimeters changes with time. One complete measurement of all four Stokes parameters  $IQUV$  requires at least four measurements of the type

$$P_i = I + a_i Q + b_i U + c_i V, \quad (\text{A1})$$

where  $P_i$  is termed the polarization state that is measured between times  $t_i$  and  $t_i + \Delta t$ . In FIRS the  $i = 1 \dots 4$  measurements are sequential in time, one complete cycle taking 1.3 sec for the data acquired here. To retrieve the quantities  $I, Q, U, V$  we must make at least four such measurements each with known values of  $a_i, b_i, c_i$  such that equation (A1) can be inverted. The modulation cycle used in the observations can be written

$$\mathbf{P} = \mathbf{M} \mathbf{S} \quad (\text{A2})$$

where  $\mathbf{S} = (I, Q, U, V)^T$ . The modulation matrix  $\mathbf{M}$  used in the observations reported here is

$$\mathbf{M} = \frac{1}{2} \begin{pmatrix} 1 & -\sqrt{3} & -\sqrt{3} & \sqrt{3} \\ 1 & -\sqrt{3} & \sqrt{3} & -\sqrt{3} \\ 1 & \sqrt{3} & -\sqrt{3} & -\sqrt{3} \\ 1 & \sqrt{3} & \sqrt{3} & \sqrt{3} \end{pmatrix} \quad (\text{A3})$$

in which  $U$  (the third column) is clearly modulated at twice the rate of  $Q, V$ . Since usually  $|I| \gg |Q|, |U|$  and  $|V|$ , two beams of light are measured for each accumulation state  $i$  with the second beam measuring  $I_i = I - a_i Q - b_i U - c_i V$ . Subtracting the two beams removes, to the level at which the beam intensities can be calibrated,  $I \rightarrow QUV$  crosstalk. Taking care of the alignment and relative gains of the two beams (dark current and flat field calibrations), the inverse matrix  $\mathbf{M}^{-1}$  applied to  $\mathbf{P}$  yields  $IQUV$  at the entrance to the polarimeter from each complete measurement cycle. To convert these measurements to the solar Stokes parameters requires inversion of a calibration matrix, taking account of the modification of the solar Stokes parameters by the telescope.

Under constant illumination, the above scheme will retrieve solar Stokes profiles to within uncertainties defined by the flat field, gain calibrations, and photon counting noise. However, if the incoming light varies on times comparable to or shorter than the accumulation cycle ( $4\Delta t$ ), systematic errors are induced. The most important time variations are probably due to atmospheric seeing, which introduces random errors proportional to the spatial gradients of the light across the solar surface (Lites 1987; Judge et al. 2004; Casini et al. 2012a). The spatial gradients are in general wavelength-dependent. If, for instance, the solar photosphere has more contrast in a line than in the neighboring continuum, seeing-induced noise will be larger in the spectral lines. When, as is usual, Stokes  $I$  is larger than  $QUV$ , variations in  $I$  are translated, by this source of measurement error, into  $Q, U$  and  $V$ . Such sources of error are termed ‘‘crosstalk’’.

In studying flares we must also be aware of time variations occurring in the solar plasma itself (Judge et al. 2004). In Paper I we found 4% changes in the IR continuum intensity in the flare footpoint, but the core intensities of the Si I and He I lines change by factors of 2 or more (see Figures 3 and 4), most likely on time scales of seconds given the RHESSI HXR observations. Under normal conditions, the He I 1083 nm multiplet forms at the base of the corona in tenuous plasma that also contributes to UV radiation. UV line and continuum brightnesses change by orders of magnitude during flares (e.g. Brekke et al. 1996). Thus we cannot discount the idea that, on time scales of seconds or less, the He I line’s intensity might change considerably. In that case, we would have to consider the possibility that the  $QUV$  profiles contain significant crosstalk from  $I$ .

The  $Q, U$  signals of a few percent exceed by at least  $20\sigma$  the random noise levels of  $\approx 8 \times 10^{-4} I_c$  (Paper I). However, *crosstalk* can induce much larger spurious polarization signals (e.g. Lites 1987). Crosstalk originates because the measurement of Stokes profiles takes time, during which at least four independent integrations in four different states of polarization must be made. In FIRS this is done sequentially in time, requiring 1.3 s for a complete cycle. If the Sun, atmospheric seeing/clouds or observing system introduces variations on time scales less than this cycle time, measured quantities contain mixtures of the average solar conditions (the ‘‘real’’ Stokes vectors sought) and other variations. When demodulated to produce the measured Stokes profiles, the profiles can contain systematic errors.

At the DST, light level and scintillation (in arc seconds) are monitored and the data are reported to the instruments. From the FIRS headers, the light levels were constant to within 1.6%. Scintillation was  $1.2'' \pm 0.35''$  (mean and rms) during the impulsive phase, slightly above the mean of  $0.88'' \pm 0.44$  of the entire scan. At wavelengths near He I 1083 nm multiplet the image intensity contrasts are also slightly higher during the flare. Therefore seeing-induced  $I \rightarrow QUV$  crosstalk cannot be immediately ruled out.

In spite of these issues we argue that the strong  $QU$  profiles observed during the flare are of solar origin, based upon several properties of the data themselves.

- Similar profiles are observed at all times throughout box ‘‘A’’ (Figure 4), under conditions of different seeing. Those shown in Figure 3 are typical profiles.



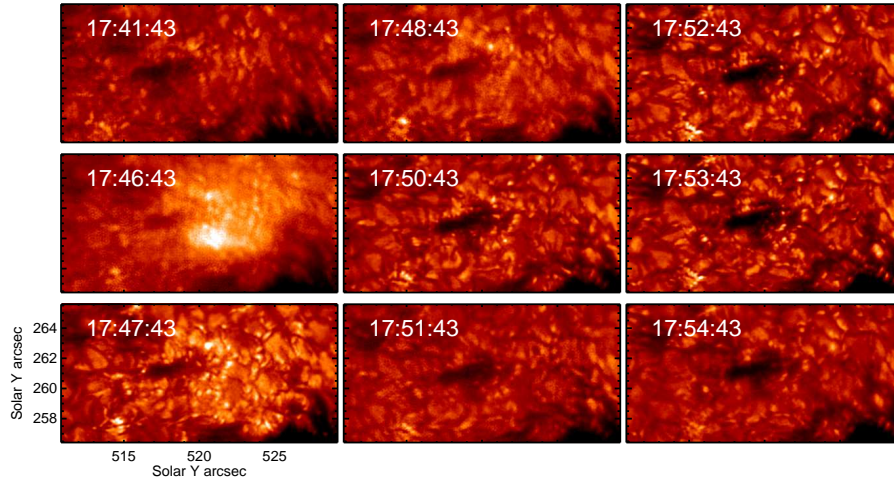


**Figure 7.** Speckle-reconstructed G-band images obtained with a CCD camera at the DST are shown, highlighting the changing quality of the atmospheric seeing during the impulsive phase of the flare ( $\approx 17:45$  to  $17:48$  UT). The “white light” flare is seen in the 17:46:43 panel.

- The impulsive phase  $QU$  profiles, while similar to Stokes  $I$ , are however not identical. Seeing-induced polarization is to a first approximation proportional to the rms seeing and spatial gradients in the solar Stokes profiles (Lites 1987). If crosstalk from  $I$  were dominating the polarization signals,  $I$ -like profiles would appear in all of  $QUV$ , for example as  $U_{\text{measured}} = U_{\text{solar}} + cI_{\text{solar}}$ . To estimate an upper limit for  $c$  we assume that all of the “sharp peak” in Stokes  $U$  near 1082.9 nm (i.e. the “blue” component) is due to crosstalk, with the measured values  $c \approx 0.005$ . Figure 3 however shows that the particular profile plotted as a line in 5 is not representative of other areas within box “A”. Indeed, both  $Q$  and  $U$  are qualitatively quite different in the lower part of box “A” from  $I$ . Thus the measured  $QU$  profiles, although they can contain some crosstalk from  $I$ , cannot be dominated by it.
- Independent reduction codes (those of S. Jaeggli, T. Schad and C. Beck) yield very similar results.

The observed behavior indicates that crosstalk in the He I 1083 nm multiplet must either be *substantially below* the  $c = 0.005$  level, or it must vary with the position along the slit. The data were acquired with the Dunn Solar Telescope’s (DST) adaptive optics system (AO) switched on. The AO system corrects for image motions mostly in an isoplanatic patch of several seconds of arc near the center of the field. The center of the AO field was close to the pore at  $X = 525''$  and  $Y = 270''$  (Kleint et al. 2015). The AO correction was of variable quality across these areas, judging from the G-band images acquired simultaneously, close-ups of which are shown in Figure 7. All things considered, we conclude that seeing-induced crosstalk does not dominate the measured  $QUV$  signals, except perhaps for the 1082.9 nm components of  $QU$  which are weaker and more susceptible to remaining systematic errors.

## B. COLLISIONAL ORIGINS OF LINEAR POLARIZATION

Anisotropic particle distributions are known to be associated with flares from *in situ* measurements in interplanetary space, and are a natural consequence of most flare particle-acceleration mechanisms (e.g., Simnett 1995). Atomic polarization is readily induced by collisions of radiating atoms with anisotropic particles (e.g., Henoux & Chambe 1990), analogously to radiation anisotropy. Given the coincidence of at least the strongest  $Q$  and  $U$  profiles with the HXR footpoint emission (Figure 1), we cannot immediately discount particle collisions as a contributing source for the observed He I 1083 nm multiplet linear polarization. Therefore here we review the basic processes by which particles may generate polarization in the He I 1083 nm multiplet.

The dominant particles in the Sun’s chromosphere are electrons, protons and hydrogen atoms. We consider terms in the Boltzmann transport equation that drive (i.e., force away from equilibrium) and relax (to equilibrium and, in particular, isotropy) the distributions of hydrogen atoms, protons, and electrons. Neutral hydrogen atoms interact only weakly with electric and magnetic fields, and the self-collisional relaxation time is short,  $\tau_{H-H} \approx (\pi a_0^2 n_H v_{\text{thermal}})^{-1} \approx 10^{-3}$  sec for  $n_H = 10^{11}$   $\text{cm}^{-3}$  (the hydrogen density varies from  $10^{11}$  to  $10^{15}$   $\text{cm}^{-3}$  across the ambient chromosphere). Note that  $\tau_{H-H} \propto \varepsilon_{\text{eV}}^{-1/2}$  where  $\varepsilon_{\text{eV}}$  is the kinetic energy in eV of the colliding particles before impact. This weak driving and strong relaxation means that hydrogen atoms are expected to be isotropic to a high degree of approximation. Impact with hydrogen can serve only to depolarize existing atomic polarization in He I.

Both electrons and protons are accelerated by electric fields, deterministic or stochastic, as such they are expected to show departures from isotropy during flares. The determination of such fields remains one of the goals of flare research (Fletcher et al. 2011). Therefore we first look at relaxation times. Relaxation self-collision times for protons and electrons are dominated by the accumulation of small angle scatterings under the long-range Coulomb potential,

and they have a different behavior with impact energy (Braginskii 1965):

$$\tau_{e-e} \approx \frac{3.5 \times 10^4 \varepsilon_{\text{eV}}^{3/2}}{(\lambda/10)n_e} \quad (\text{B1})$$

$$\tau_{p-p} \approx \frac{2 \times 10^6 \varepsilon_{\text{eV}}^{3/2}}{(\lambda/10)n_p} \quad (\text{B2})$$

where  $\lambda$  is the Coulomb logarithm (between 10 and 35 for most plasma in the solar atmosphere),  $n_{e,p}$  are ambient electron and proton densities. With  $n_e = n_p \gtrsim 10^{11} \text{ cm}^{-3}$  throughout the chromosphere we find collision times of  $\lesssim 10^{-7} \varepsilon_{\text{eV}}^{3/2}$  and  $\lesssim 10^{-5} \varepsilon_{\text{eV}}^{3/2}$  sec for electrons and protons respectively. To retain an anisotropic distribution function, the particles that impact helium atoms must survive collisional relaxation on their journey from the source of acceleration into plasmas emitting the helium spectrum. This constraint would seem to rule out particles at low energies. The accumulations of many Coulomb collisions leads to a stopping or penetration depth in column mass units, such that, for electrons

$$m_p = 1.4 \times 10^{-5} \times \left(\frac{\varepsilon_{\text{keV}}}{20}\right)^2 \text{ g cm}^{-2} \quad (\text{B3})$$

This leads to a constraint ‘‘C1’’, a lower limit on the energy of particles that can travel through the chromosphere. In the standard model, the pre-flare chromosphere is at column masses of  $\gtrsim 10^{-5} \text{ g cm}^{-2}$ , so that only electrons of energy  $\gtrsim 20 \text{ keV}$  or protons of energy  $\gtrsim 1 \text{ MeV}$  can enter the chromosphere from above and retain some anisotropy.

To generate significant polarization in neutral atoms by electron or proton collisions requires an anisotropic particle distribution at energies  $\varepsilon$  where the absolute cross sections  $\sigma(\varepsilon)$  are sufficiently large (constraint ‘‘C2’’), and where the cross sections for the magnetic sub-states are also sufficiently different (constraint ‘‘C3’’) such that sub-state populations become unequal. For inelastic collisions (ionization, recombination, collisional excitation and de-excitation), C2 and C3 occur together only under rather restrictive conditions. Further, these conditions are generally in conflict with C1.

For electron-ion collisions, consider the recombination process

$$1s^2 S_{1/2} + e^-(\varepsilon, \ell = 1) \rightarrow 1s2p^3 P_{2,1,0}^o + h\nu \quad (\text{B4})$$

and similar processes for recombination to higher levels ( $1snl$  configurations,  $n > 2$ ) which cascade down the triplet system of helium. Here,  $\varepsilon$  is the average energy of electrons with angular momentum  $\ell$ . The cross sections for this process are relatively small (compared with other collisional processes), yielding rates of recombination per  $\text{He}^+$  nucleus that are  $\approx 10^{-13} n_e \varepsilon_{\text{eV}}^{-1/2} \text{ s}^{-1}$ , using hydrogenic coefficients from (Allen 1973, §38). The conflict of constraint C1 with C2 is evident. *Recombination is improbable at the energies where electrons survive long enough to maintain anisotropic distribution functions.*

For collisional excitation, we use the theory of impact polarization by Percival & Seaton (1958) to estimate differential cross sections for collisions between different sub-levels (with magnetic quantum number  $M$ ). In the absence of electron exchange (which is usually negligible for electric dipole transitions, varying as  $\varepsilon^{-3}$  (Seaton 1962; Burgess & Tully 1992) and ignored in the Percival-Seaton theory), the collision cross sections are determined by the impacting particle’s path and charge. For neutral targets, the paths of electrons and protons are essentially the same (at least at energies greatly in excess of the 1-10 eV bound energies), being represented by plane waves and an outgoing spherical wave. Thus the cross sections for protons should be very close to those computed using the theory for electrons. The only long-lived level from which collisions with energetic particles might directly excite and polarize the He I 1083 nm multiplet is  $1s2s^3 S_1$ , the other long lived He I levels requiring spin changing transitions with small cross sections. Therefore, we consider the process

$$1s2s^3 S_1 + e^-(\varepsilon, \ell) \rightarrow 1s2p^3 P_{2,1,0}^o + e^-(\varepsilon', \ell' = \ell \pm 1) \quad (\text{B5})$$

Collisions to the  $1s2p^3 P_{2,1,0}^o$  upper levels occur via electric dipole transitions, for which the collision cross section varies as (Seaton 1962)

$$\sigma \propto \frac{\ln \varepsilon}{\varepsilon} \quad (\text{B6})$$

Constraint C2 is in conflict with C1 again: At very high energies the probability of exciting the  $1s2p^3 P_{2,1,0}^o$  upper levels drop rapidly with increasing energy. The differential cross sections of Percival & Seaton (1958) at very high energies can be estimated using the Born approximation (Section 6 of Percival & Seaton 1958). The cross sections maintain the same differential atomic polarization (i.e. constraint C3). We conclude for the He I 1083 nm multiplet that there is a ‘‘sweet spot’’ in energy such that the cross sections for generating large populations are large (C2, low-ish energy) but that the energies are sufficiently high (C1) that the impacting electrons or protons penetrate the chromosphere and remain anisotropic.

Figure 8 shows the cross sections computed using the theory of Percival & Seaton (1958) using cross section data computed from Flannery & McCann (1975). The right hand panel shows the net polarization induced by collisions with electrons and protons, parallel and perpendicular to a collimated beam of such particles. For electrons, constraints C1 forces us to adopt a population of electrons with energies  $\gtrsim 20 \text{ keV}$ . But at such energies the cross sections become

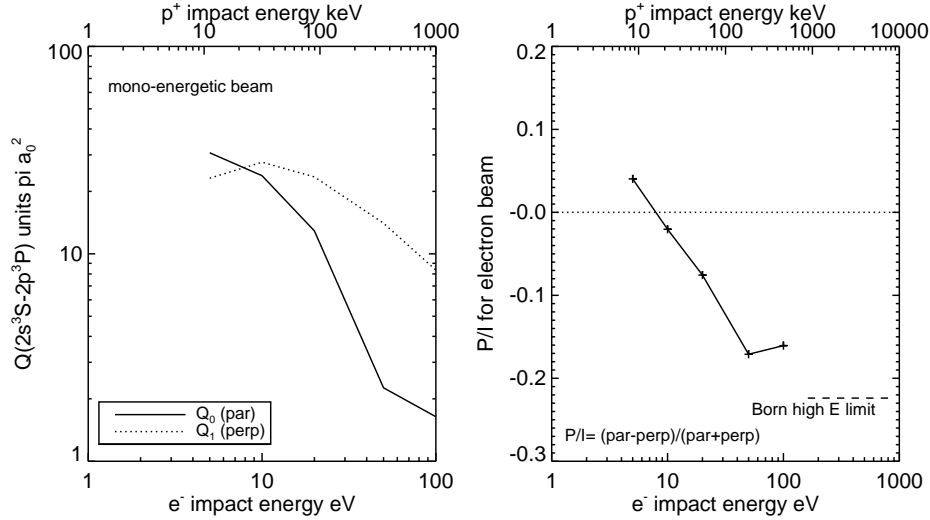


**Figure 8.** The left panel shows cross sections computed as a function of energy for the excitation of parallel and perpendicular components of the He I 1083 nm multiplet. (The reference direction is the direction of the peak of the particle distribution function, a beam in this case). The sum of the cross sections gives the usual total cross section for excitation from the long-lived  $1s2s\ ^3S_0$  level in He I. The right panel shows the energy dependence of the ratio of these components, related to the net linear polarization and its sign.

very small (as seen through extrapolation of the left panel of Figure 8 using Equation (B6)). The left hand panel of the figure shows that a population of protons above 1 MeV (C1) might satisfy constraints C2 and C3. In words, MeV protons might just account for the observed polarization in the 1083.0 nm transitions.

Note however that this theory produces polarization *only* in the two 1083.0 nm transitions whose upper levels are polarizable ( $J = 1$  and  $2$ ). In the main text we emphasize the need for *lower level* polarization to produce polarization in the 1082.9 nm line which has an unpolarizable ( $J = 0$ ) upper level. To populate this level at all, let alone polarize it, one requires an electron exchange transition from level (1) or recombination from level (3). In either case the probability of generating a polarized lower level, independent of the radiation field, is small. Thus we conclude that collisions are not the primary source of the observed polarization.

## REFERENCES

- Allen, C. W. 1973, *Astrophysical Quantities* (Univ. London: Athlone Press)
- Allred, J. C., Hawley, S. L., Abbett, W. P., & Carlsson, M. 2005, *Astrophys. J.*, 630, 573
- Benz, A. O. 2008, *Living Reviews in Solar Physics*, 5, 1
- Bianda, M., Benz, A. O., Stenflo, J. O., Küveler, G., & Ramelli, R. 2005, *Astron. Astrophys.*, 434, 1183
- Braginskii, S. I. 1965, *Reviews of Plasma Physics.*, 1, 205
- Brekke, P., Rottman, G. J., Fontenla, J., & Judge, P. 1996, *Astrophys. J.*, 468, 418
- Brown, J. C. 1971, *Solar Phys.*, 18, 489
- Burgess, A., & Tully, J. A. 1992, *Astron. Astrophys.*, 254, 436
- Carmichael, H. 1964, *NASA Special Publication*, 50, 451
- Carrington, R. C. 1859, *Mon. Not. R. Astron. Soc.*, 20, 13
- Casini, R., de Wijn, A. G., & Judge, P. G. 2012a, *ApJ*, 757, 45
- Casini, R., Judge, P. G., & Schad, T. A. 2012b, *Astrophys. J.*, 756, 194
- Casini, R., & Landi Degl'Innocenti, E. 2008, *Plasma Polarization Spectroscopy*, ed. T. Fujimoto & A. Iwamae (Springer), 247
- Fano, U. 1957, *Reviews of Modern Physics*, 29, 74
- Flannery, M. R., & McCann, K. J. 1975, *Journal of Physics B Atomic Molecular Physics*, 8, 1716
- Fletcher, L., Hannah, I. G., Hudson, H. S., & Metcalf, T. R. 2007, *Astrophys. J.*, 656, 1187
- Fletcher, L., Dennis, B. R., Hudson, H. S., et al. 2011, *Space Sci. Rev.*, 159, 19
- Hale, G. E. 1931, *Astrophys. J.*, 73, 379
- Hanaoka, Y. 2003, *ApJ*, 596, 1347
- Heinzel, P., & Kleint, L. 2014, *Astrophys. J. Lett.*, 794, L23
- Henoux, J. C., & Chambe, G. 1990, *J. Quant. Spectrosc. Radiat. Transfer*, 44, 193
- Henoux, J. C., Chambe, G., Smith, D., et al. 1990, *Astrophys. J. Suppl. Ser.*, 73, 303
- Hirayama, T. 1974, *Sol. Phys.*, 34, 323
- Holman, G. D., Aschwanden, M. J., Aurass, H., et al. 2011, *Space Sci. Rev.*, 159, 107
- Hurford, G. J., Schmahl, E. J., Schwartz, R. A., et al. 2002, *Solar Phys.*, 210, 61
- Jaeggli, S. 2011, PhD thesis, University of Hawaii
- Jefferies, J., Lites, B., & Skumanich, A. 1989, *Astrophys. J.*, 343, 920
- Judge, P. G., Elmore, D. F., Lites, B. W., Keller, C. U., & Rimmele, T. 2004, *Applied Optics: optical technology and medical optics*, 43, issue 19, 3817
- Judge, P. G., Kleint, L., Donea, A., Sainz Dalda, A., & Fletcher, L. 2014, *Astrophys. J.*, 796, 85
- Kerr, G. S., & Fletcher, L. 2014, *Astrophys. J.*, 783, 98

- Kleint, L., Battaglia, M., Reardon, K., et al. 2015, *Astrophys. J.*, 806, 9
- Kopp, R., & Pneuman, G. 1976, *Sol. Phys.*, 50, 85
- Kuckein, C., Collados, M., & Manso Sainz, R. 2015a, *Astrophys. J. Lett.*, 799, L25
- Kuckein, C., Collados, M., Manso Sainz, R., & Asensio Ramos, A. 2015b, ArXiv e-prints
- Landi Degl'Innocenti, E., & Landolfi, M. 2004, *Astrophysics and Space Science Library*, Vol. 307, Polarization in Spectral Lines
- Lin, R. P., Dennis, B. R., Hurford, G. J., et al. 2002, *Solar Phys.*, 210, 3
- Lites, B. W. 1987, *Applied Optics*, 26, 3838
- Lites, B. W. 2000, *Reviews of Geophysics*, 38, 1
- Mihalas, D. 1978, *Stellar Atmospheres* (San Francisco (second edition): W. H. Freeman and Co.)
- Newton, H. W. 1930, *Mon. Not. R. Astron. Soc.*, 90, 820
- Percival, I. C., & Seaton, M. J. 1958, *Royal Society of London Philosophical Transactions Series A*, 251, 113
- Seaton, M. J. 1962, in *Atomic and Molecular Processes*, ed. D. R. Bates (New York: Academic Press), 11
- Simnett, G. M. 1995, *Space Sci. Rev.*, 73, 387
- Stenflo, J. O., Bianda, M., Keller, C. U., & Solanki, S. K. 1997, *Astron. Astrophys.*, 322
- Štěpán J., Heinzel P., 2013, *ApJ* 778, L6
- Sturrock, P. A. 1966, *Nature*, 211, 695
- Trujillo Bueno, J., Landi Degl'Innocenti, E., Collados, M., Merenda, L., & Manso Sainz, R. 2002, *Nature*, 415, 403